Lab on a Chip

An optoelectrokinetic technique for programmable particle manipulation and bead-based biosignal enhancement

Journal:	*Lab on a Chip*
Manuscript ID:	LC-ART-06-2014-000661.R2
Article Type:	Paper
Date Submitted by the Author:	22-Jul-2014
Complete List of Authors:	Wang, Kuan-Chih; National Cheng Kung University, Department of Biomedical Engineering Kumar, Aloke; University of Alberta, Department of Mechanical Engineering Williams, Stuart; University of Louisville, Mechanical Engineering Green, Nicolas; University of Southampton, School of Electronics and Computer Science Kim, Kyung-Chun; Pusan National University, School of Mechanical Engineering Chuang, Han-Sheng; National Cheng Kung University, Department of Biomedical Engineering

An optoelectrokinetic technique, termed Rapid Electrokinetic Patterning (REP), was used to enhance the signal in bead-based bioassays. REP can achieve various manipulation capabilities, such as micro/nano-particles aggregation, translation, sorting, single particle trapping, and patterning.

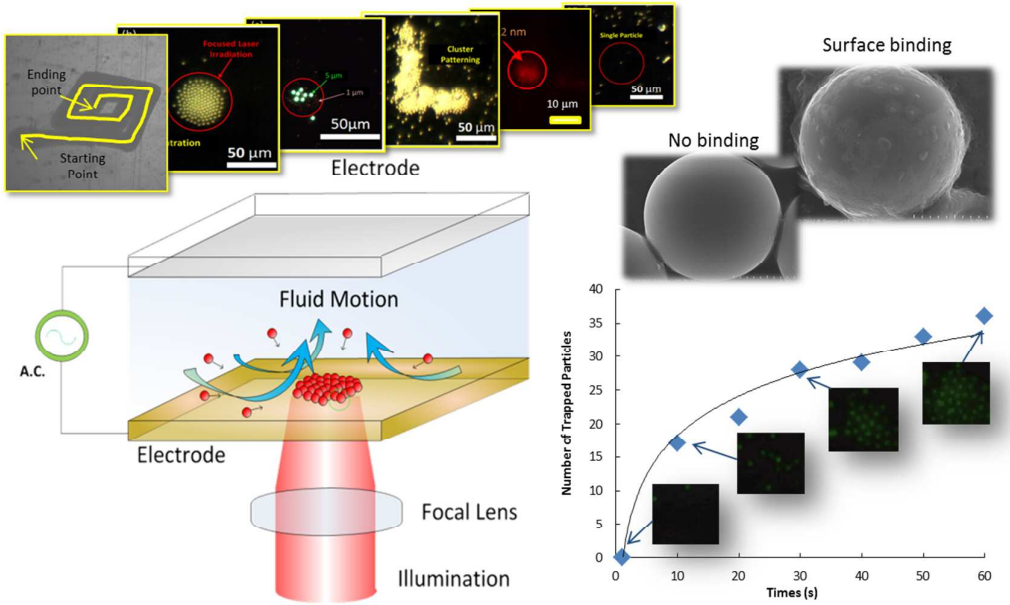

An optoelectrokinetic technique for programmable particle manipulation and bead-based biosignal enhancement

Kuan-Chih Wang[a], Aloke Kumar[c], Stuart J. Williams[d], Nicolas G. Green[e], Kyung Chun Kim[f], and Han-Sheng Chuang*[a,b]

Received (in XXX, XXX) Xth XXXXXXXXX 201X, Accepted Xth XXXXXXXXX 201X

First published on the web Xth XXXXXXXXX 201X

DOI: 10.1039/b000000x

Abstract

Technologies that can enable concentration of low-abundance biomarkers are essential for early diagnosis of diseases. In this study, an optoelectrokinetic technique, termed Rapid Electrokinetic Patterning (REP), was used to enable dynamic particle manipulation in bead-based bioassays. Various manipulation capabilities, such as micro/nano-particles aggregation, translation, sorting and patterning, were developed. The technique allows for versatile multi-parameter (voltage, light intensity and frequency) based modulation and dynamically addressable manipulation, with simple device fabrication. Signal enhancement of a bead-based bioassay was demonstrated using dilute biotin-fluorescein isothiocyanate (FITC) solutions mixed with streptavidin-conjugated particles and rapidly concentration with the technique. As compared with a conventional ELISA reader, the REP-enabled detection achieved a minimal readout of 3.87 nM, which was a 100-fold improvement in sensitivity. The multi-functional platform provides an effective measure to enhance detection levels in more bead-based bioassays.

Keywords: REP, optoelectrokinetic manipulation, particle, microfluidics, bead-based bioassay, optofluidics

Introduction

Diagnostics are critical to early detection of diseases and they play a pivotal role in today's health care. Amongst various diagnostic techniques, bead-based bioassays have drawn significant attention in recent years due to its simplicity as well as broad applications.[1-3] Bead-based bioassays, as opposed to conventional bioassays, feature not only simplicity but also flexibility and programmability. Lab-on-chip (LOC) systems are

key to enabling point-of-care diagnostics and this has led to several investigations on incorporating bead-based assays in LOC systems. Thompson et al.[4] immobilized streptavidin-coated agarose beads to collect dispersed biotinylated quantum dots in a microchannel. However, their system was diffusion-limited requiring hours for detection. Yu et al.[5] designed a microfluidic bead-based immunoassay for multiplexed detection of proteins. The benefits of the device are small quantities of samples and simultaneous determination of a multitude of parameters. The authors used valves for fluid pumping to enable a reduced assay time as compared what would be possible due to diffusive transport alone. Non-invasive manipulation techniques for controlling transport in such LOC based immunoassay systems have also been implemented. Dielectrophoresis (DEP) has been widely applied in a wide variety of bead-based bioassays,[6-9] and offer several advantages such as ability to differentiate between particles of different types. However, DEP is limited in its implementation due to the use of fixed electrodes. Optical tweezers (OTs), which utilize optical pressure to manipulate particles, have also been used for immunoassays.[10-12] OTs demonstrate programmability and user-defined positioning of beads.

The recent advent of optoelectrokinetic techniques for non-invasive manipulation in systems introduces a new paradigm for the control of analytes in microfluidic systems.[13-16] REP is a recently discovered technique, which has been demonstrated to be capable of high throughput and programmable technique for particle manipulation.[17-20] REP typically utilizes a parallel plate electrode system and a highly focused laser beam to create localized 'hot-spots' on the electrodes. The localized hot-spots lead to electrothermal flows,[21] which allow for rapid collection of analytes as a desired location on the electrode.

In this study we demonstrate a high-throughput, programmable bioassay enabled by REP. The microchip was composed of an ITO glass cover (top) and a glass slide coated with a gold film (bottom). Both glass plates were separated by a spacer (50 μm thickness) (Fig. 1a). A power adjustable IR laser (1064 nm, 300 mW) was focused on the bottom side of the microchip. An upright microscope coupled with a fast CMOS camera was used to visualize and record the manipulation (Fig. 1b). A motorized mirror was incorporated into the optical pathway to enable the reaction spot to sweep over the entire microchip to further concentrate dispersed analytes (Movie S1). The arrangement promotes efficiency of the REP-enabled detection. An ELISA reader, a well-adopted instrument for bioassay quantifications, was used to compare with REP.

The bioassay was realized by the biotin-streptavidin reaction, whose binding strength approaches a covalent bond.[22] The greatest benefits of the reaction are enhanced speed and simplicity during an assay development. To facilitate the optical detection, biotin was tagged with the fluorescent dye, FITC, while streptavidin was conjugated on the surfaces of 6-μm polystyrene particles. In a normal assay biotin-streptavidin binding is usually diffusion limited. However, we demonstrated that REP can significantly enhance the reaction kinetics to allow effective detections of binding events at very low concentration levels. Efficiency of REP-driven assays was compared with that of an ELISA reader. The minimal readout of the biotin concentration of REP reached 3.87 nM while that of the ELISA reader reached only 387 nM. Our work shows that REP can serve as a useful tool for bioassays and can potentially be applied to detect low concentration biomarkers that are beyond the sensitivity limits of conventional techniques.

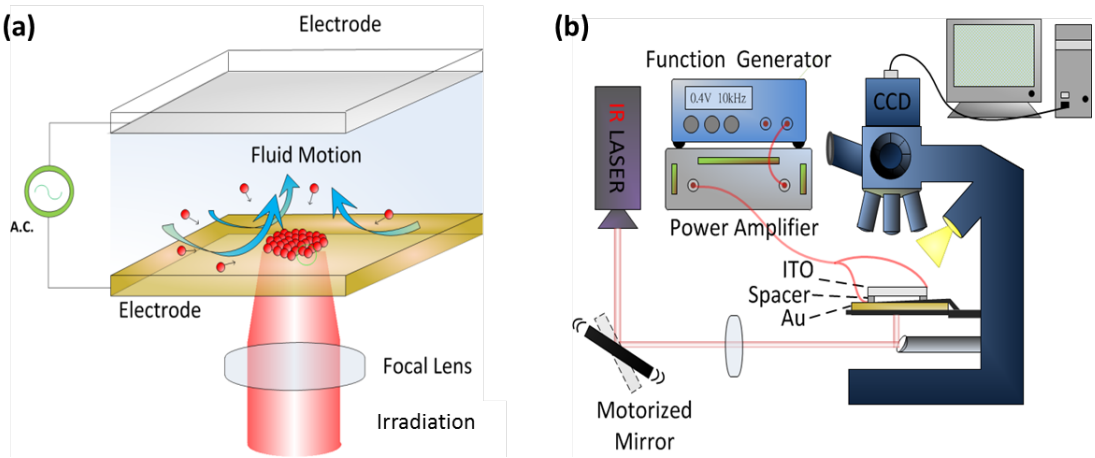

Fig. 1: *(a) Illustration of the optoelectrokinetic trapping system. (b) Schematic of the experimental setup.*

Materials and Methods

Optoelectrokinetic Effect

An empirical model elucidating the relationship of forces is shown in Fig. 2. To be consistent with the experiment, the conductivity of the medium in the model was assumed to be 0.3 mS m^{-1}. Table 1 shows a list of relationships between forces and frequencies. From a global viewpoint (Fig. 2a), electrothermal and AC electroosmotic (ACEO) effects drive the fluid toward the center of irradiation, resulting in a toroidal flow. Consequently, particles are brought to the center by the fluid drag force (F_{drag}). The location of trapped particles

can be dynamically altered with the irradiated spot. The electrothermal flow herein is a result of heating from external irradiation in the presence of electric fields. The heating induces gradients of conductivity and permittivity in the liquid medium so that ions are moved in the fluid bulk. The time-averaged expression for this electrothermal body force is [23]

$$\langle f_e \rangle = 1/2Re\left[\frac{\sigma_m \varepsilon_m(\alpha-\beta)}{\sigma_m + i\omega\varepsilon_m}(\nabla T \cdot E)E^* - 1/2\varepsilon_m \alpha |E|^2 \nabla T\right], \quad (1)$$

where * indicates complex conjugate and *Re* refers to the real part of expression; for an AC signal of frequency ω, E is the electric field; σ_m and ε_m are the conductivity and permittivity of fluid, respectively; β and α are $(1/\sigma_m)(\partial\sigma_m/\partial T)$ and $(1/\varepsilon_m)(\partial\varepsilon_m/\partial T)$, respectively. The equation indicates that a temperature gradient is more important than an absolute temperature in the electrothermal flow. The first term in Equation (1) represents the Coulomb force and the second term represents the dielectric force. A high laser intensity (*i.e.*, a high temperature gradient) enhances the electrothermal flow, whereas an increased AC frequency diminishes the effect as it approaches its charge relaxation (ε_m/σ_m). Electrothermal flow speed decreases significantly when the applied frequency crosses the upper limit (>f_H)[24], and for practical purposes flow can be considered negligible.

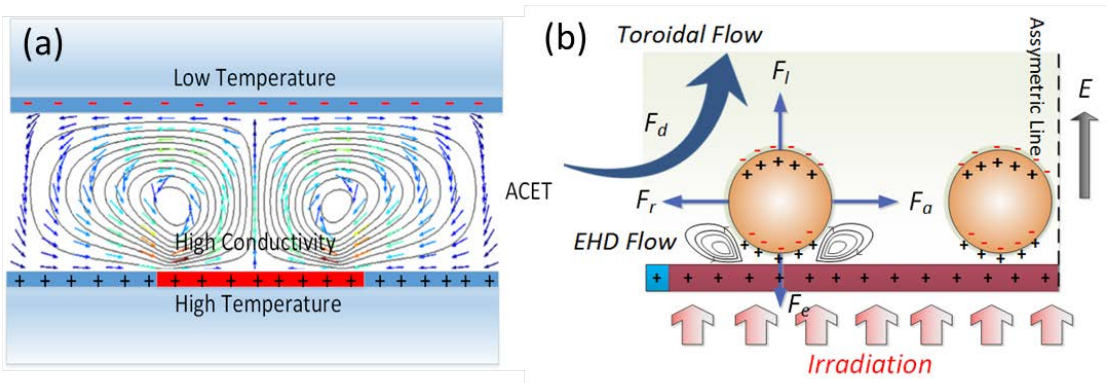

Fig. 2: *The optoelectrokinetic model (a) in global viewpoint – toroidal flow and (b) in local viewpoint – particle-particle/electrode interactions.*

Table 1: *A summary of force analysis in the empirical model.*

	Global Viewpoint	Local Viewpoint			
	F_{drag}	F_a	F_e	F_r	F_l
$<f_L$	Strong Electro-thermal	Strong Local EHD	EDL & Gravity*	ED	Strong Electro-thermal
f_L~f_M	Declining Electrothermal	Weak Local EHD	Weak EDL, MW & Gravity	Weak EDL & MW	Declining Electrothermal
f_M~f_H	Weak Electrothermal	None	MW & Gravity	MW	Weak Electrothermal
$>f_H$	None	None	MW & Gravity	MW	None

* The effect of gravity grows as the particle size increases. Here the gravity is comparable to F_l for 10 μm

From a local viewpoint, the optoelectrokinetic behavior of particles during aggregation is a dynamically balanced state of multiple electrokinetic force interactions. To facilitate the analysis, all forces are simplified to four types as illustrated in Fig. 2b. F_l herein denotes a lift force capable of moving particles away from the bottom electrode. The lift force is a combination of several complex phenomena: (i) the bulk electrothermal vortex, (ii) hydrodynamic lift when a particle is close to a wall, (iii) the disruption of bulk flow in particle aggregates, and (iv) localized, particle-electrode induced hydrodynamic flow. Particle-particle repulsive electrokinetic interactions (*i.e.*, the dipole-dipole repulsive force) may also lift particles if the particle aggregation becomes more compact, generating instability within the aggregation. Prior study[24] showed that the bulk electrothermal flow is the major contributor to F_l and declines exponentially with frequency, so the force reaches the maximum at low frequencies ($<f_L$) but becomes negligible when exceeding the upper limit frequency ($>f_H$). F_a denotes the particle-particle attraction, which is dominated by the local electrohydrodynamic (EHD) flow at low frequencies ($<f_L$).[25, 26] Although the electric field seems to be uniform between the two electrodes of the optoelectric device, the local electric fields adjacent to particles are distorted by the particle itself inducing the non-uniform fields for local EHD flow. The tiny vortices bring particles toward each other and levitate them slightly above the surface of electrode.[27] F_r and F_e denote the particle-particle repulsion and the particle-electrode adhesion, respectively. The induced dipoles form repulsion between particles when particles are perpendicular to the electric

field, but turn to attraction when particles are aligned in parallel with the electric field regardless of frequency.[28] These phenomena elucidate why particles repel each other but are attracted to the surface of the electrode in the presence of electric fields. Since F_e decays rapidly with distance, trapped particles stay near the bottom surface. Instead of adhesion, particles float slightly above the bottom surface due to the local EHD flow. All the three forces, F_a, F_r, and F_e, at the low frequency domain ($<f_L$), are subjected to the electric double layer (EDL) polarization. Similar to the electroosmotic flow, the EDL induced forces peak at low frequencies but diminishes when the frequency is over f_L. The EDL polarization dispersion is attributed to ions within the double layer incapable of migrating around particles as fast as the polarized electric field. With the relaxation of EDL polarization the Maxwell-Wagner (MW) induced forces (*a.k.a.*, dielectrophoretic effect) take over. In the transitional phase (f_L~f_M), F_a, F_r, and F_e decline significantly due to the transition from EDL polarization to MW polarization. Since the electrothermal flow induced force (F_l) declines slower than the MW induced particle-electrode adhesion (F_e), particles cannot be trapped firmly on the electrode. The provisional imbalance accounts for the disappearance of particle aggregation during the frequency period. When the frequency is between f_M and f_H, however, the electrothermal flow is constantly declining, leaving F_r to drop below F_e. The reversal relationship between F_l and F_e hence allows particle to re-aggregate. Unlike the trapping at low frequencies, the re-aggregation is loose and weak due to lack of the local EHD induced attraction (F_a) and weak electrothermal flow. It was also observed that gravity induced particle sedimentation appeared to be significant, particularly for 10 μm particles, because the toroidal flow is incapable of inducing strong drag to lift the particles. Eventually when the frequency is over f_H, the optoelectrokinetic trapping is terminated due to extinction of electrothermal flow even though the MW induced forces remain effective.

Operation of the Optoelectric System

Before operation, a microchip was fixed on a holder with edges of ITO glass and gold electrode connected to the power amplifier. A function generator (GFG-3015, GWINSTEK) was used to provide a sinusoidal signal to the power amplifier (2340, TEGAM). A tunable solid-state IR laser beam (300 mW, 1064 nm, LD-WL206, Optoelectronics Tech.) was directed to the bottom of the microchip and focused on the back of the gold electrode. A motorized mirror (T-MM2, Zaber Technologies) was set up in the light path to steer the laser beam

for programmable particle trapping. Above the microchip, an upright fluorescent microscope (BX51, Olympus) was used to visualize the particle manipulation. A 10X objective lens, a proper filter cube, and a fast CMOS camera (FL3-03-13S2C-CS, PointGrey) were used to capture particle images. For measuring temperature distributions of the microchip, an IR coated microscope coupled with an IR camera (IRM-P320G-10μm, Ching-Hsing Computer Tech.) was instead used. When operating the system, the electric field was usually applied firstly and then the laser beam was activated to start the optoelectrokinetic trapping.

Materials

Fluorescent polystyrene particles were purchased from Thermo Fisher Scientific. The particle sizes used in the study were 1 μm, 3 μm, 5 μm, and 10 μm. All particle suspensions were prepared in a concentration of 3.7×10^8 count mL^{-1} by diluting with DI water. The conductivity of particle suspension was measured prior to each manipulation to ensure consistency. Titration by mixing with phosphate buffered saline (1X PBS) was taken to slightly adjust the conductivity to 0.3 mS m^{-1}. ITO glass was purchased from Sigma-Aldrich and trimmed to a size of 50 mm × 50 mm. A gold electrode was fabricated by coating a layer of 150-nm gold film and a 25-nm Cr adhesive layer on a glass slide using an E-beam evaporator. The microchip was eventually assembled by clamping an ITO glass and a gold electrode with paper clips. Scotch® Tape (55 μm, 3M) was used as a spacer between the ITO glass and the gold electrode. To reuse the microchip, both the ITO glass and gold electrode were rinsed with ethanol and deionized water for a few times, and then sonicated in acetone for 10 minutes.

For the demonstration of signal enhancement in a bioassay, streptavidin-conjugated particles (6 μm, #24158, Polyscience) and FITC tagged biotin (FL-53608, Sigma-Aldrich) were used. Conductivity was maintained approximately at 0.3 mS m^{-1}.

Results and Discussions

Characterization of the Optoelectrokinetic Trapping

The temperature gradient in the device was generated by a focused laser beam. As mentioned previously, the irradiated spot was a virtual electrode to the trap particles. Fig. 3 shows the temperature distributions before and after irradiation measured by a microscopic IR camera. With an electric field only, the temperature was uniformly maintained at 32 °C while the room temperature was 28 °C. Conversely, a normal distribution peaking at nearly 39 °C took shape after irradiation under the laser intensity of 69 W cm^{-2}.

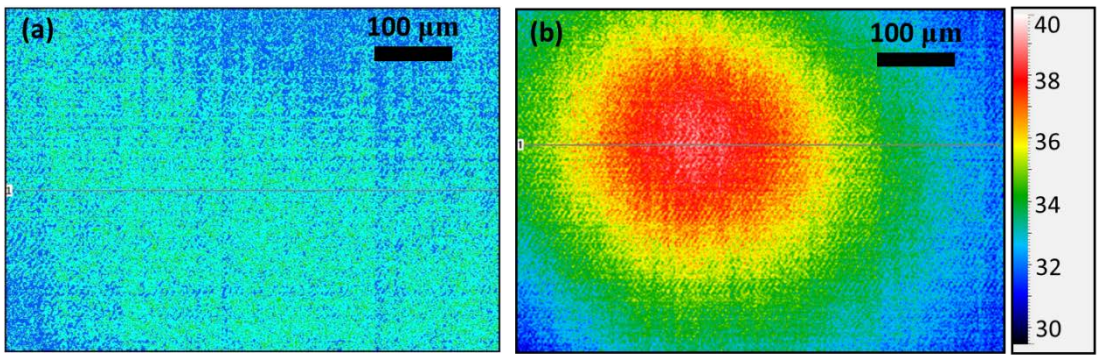

Fig. 3: *Temperature distributions (a) with and (b) without laser irradiation. The temperature scale is in Celsius.*

Taking all the electrohydrodynamic and electrokinetic effects into consideration, the possible scenarios of particle behavior and frequency in the optoelectric device summarized in Table 1 are verified in the experiments (Fig. 4). At low frequencies ($<f_L$), particles are brought to the irradiated spot by the toroidal electrothermal flow (Fig. 4a) and then form a compact cluster by the particle-particle attraction resulting from the local EHD flow (Fig. 4d). At the transitional phase ($f_L \sim f_M$), effective particle trapping temporarily disappears due to the diminishing EDL polarization and the MW relaxation frequency (Fig. 4e) even though the globally electrothermal flow remains effective (Fig. 4b). When the frequency enters the interval $f_M \sim f_H$, particles slowly re-aggregate to form a cluster (Fig. 4c). However, the cluster structure in this frequency domain is usually less dense due to lack of the particle-particle attractive force (F_a) to resist the repulsive force (F_r) (Fig. 4f). In addition, the declining electrothermal flow accounts for the slow response. When the frequency exceeds the upper limit ($>f_H$), toroidal flow becomes negligible, resulting in no optoelectrokinetic trapping. Consequently, the result suggests the optimal range of optoelectrokinetic trapping to be the low frequencies ($<f_L$) rather than the frequency interval between f_M and f_H.

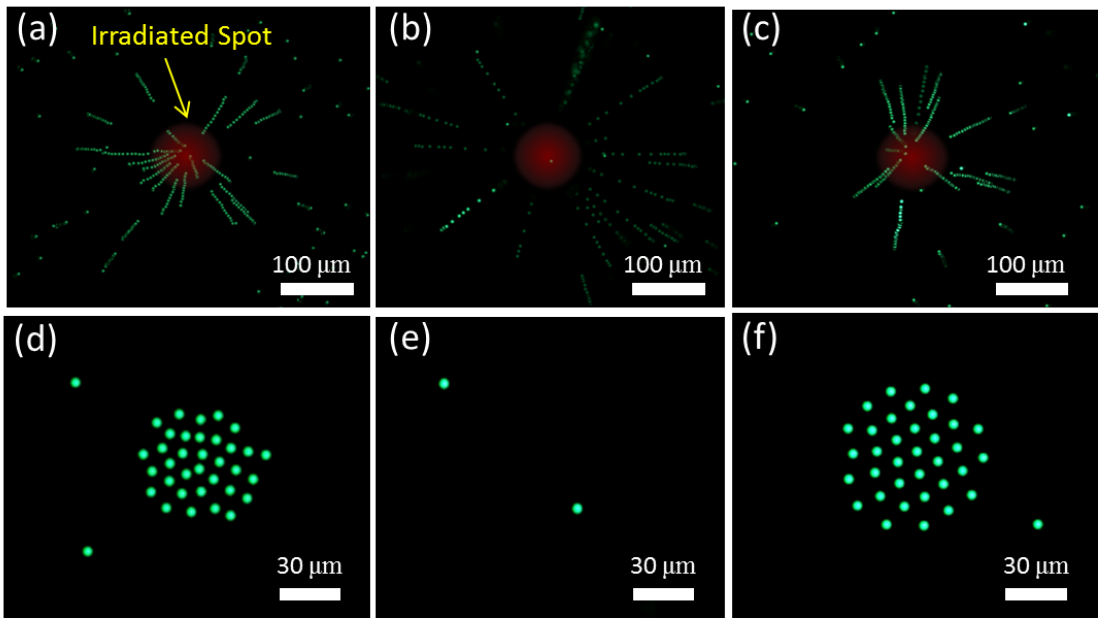

Fig. 4: *Multiple exposures of 5-μm particle trajectory at (a) 5 kHz, (b) 100 kHz, and (c) 1 MHz. Close-ups of 5-μm particle cluster at (d) 5 kHz, (e) 100 kHz, and (f) 1 MHz.*

To verify the model, laser intensity, voltage, and frequency were investigated. Fig. 5a shows the measured optoelectrokinetic behavior of particles with respect to different frequencies. Frequencies ranging from 5 kHz to 5 MHz were conducted. All particles appeared to experience distinct responses at different frequency domains as predicted in the model. The frequency domains varied with particle size as well. The observed responses were divided into four zones, including strong trapping, no trapping with vortices, weak trapping, and no trapping without vortices. In general, between 1 kHz and f_L (the green solid line), a dense cluster was achieved. Below 1 kHz, bubbles were formed, signifying electrolysis due to Faradaic reactions. Accordingly, the minimal frequency investigated was chosen to be 5 kHz in the study. Between the green solid line and the red dotted line (f_L~f_M), no particles were firmly trapped. When the frequency was over the red dotted line ($>f_M$) but remained below the upper limit ($<f_H$), a loose cluster reappeared. The electrothermal flow disappeared when the frequency exceeded the upper limit ($>f_H$). No effective aggregation was ever observed beyond the upper limit. As mentioned previously, gravity contributes additional effect to F_e in larger particles, resulting in 10 μm particles to be trapped at all frequencies. The right insets of Fig. 5a show the actual particle images of 5 μm

particles captured at 5 kHz, 20 kHz, 100 kHz, and 2 MHz (also see Movie S2). A good agreement with the prediction validates the hypothetical model.

In addition to the validation, three novel observations were made: (1) single particle trapping, (2) smallest nano-particle trapped by REP, and (3) re-aggregation at high frequencies. The single particle trapping occurred near the two transitional boundaries (*i.e.*, f_L and f_M). We found that particles tended to detach from a cluster when approaching f_L but re-aggregated when approaching f_M. Therefore, the single particle trapping can be achieved by carefully tuning the frequency near the two critical values. REP has been proven not only powerful in micro-particle trapping but also in nano-particle trapping.[19] A clump of 22 nm polystyrene particles was successfully aggregated in this study. The size is the smallest record that REP has ever demonstrated to date. Additionally, in an early attempt to trap other nano-sized materials, such as gold nanoparticles and quantum dots (CdSe), excellent aggregation was observed as well, showing the potential applications at the nanoscale. The Re-aggregation behavior at high frequencies was also observed (Fig. 5a). In our model this behavior is likely a result of reduced hydrodynamic lift (F_l) due to the declining electrothermal flow. A simple test by switching off either electric fields or laser resulted in disaggregation, confirming the necessity of applying laser and electric fields simultaneously. The test implied that the optoelectrokinetic trapping remained effective in the high frequency domain. However, the trapping progressively weakened as the frequency approached the upper limit (f_H).

In addition to the frequency, the particle trapping is also a function of voltage and laser intensity (Fig. 5b). Unless mentioned otherwise, 5 μm polystyrene particles prepared in a concentration of 3.7×10^8 count mL^{-1}, 1064 nm IR laser, 5 kHz, and 0.3 mS m^{-1} medium were used for all measurements in the study. To facilitate the assessment of particle trapping, concentration efficiency (CE) was introduced. The CE index was defined as the number of particles aggregated within the irradiated spot in a second. Therefore, a high CE value means a large aggregate in a short period of time and vice versa. When the laser intensity is elevated, the CE index increases accordingly. The increase usually comes along with strong toroidal flow. Similarly, the CE index increases as the voltage is elevated as well. The toroidal flow is subjected to the modulated electric field. The strong vortices promote the particle aggregation by bringing more particles to the center of irradiation rapidly.

However, high voltages may cause electrolysis and electric breakdown while high laser intensity usually causes overheat.

Light intensity affects not only the CE index but also the mean distance (λ_p) between particles. In the trapping zone at low frequencies ($<f_L$), λ_p increases with the light intensity (Fig. 5c and Movie S3). Since conductivity is proportional to temperature, high light intensity suppresses the particle-particle attraction due to dwindling local EHD flow, repelling particles from each other. Compared with the EDL induced repulsive force, the electrothermal flow is insignificant. Whereas, λ_p decreases with the light intensity in the trapping zone between f_M and f_H (Fig. 5d and Movie S4). When the light intensity is over 291 W cm^{-2}, however, all particles collapse to the center as shown in the inset (vii) of Fig. 5d. Unlike the dominant attraction at low frequencies, no significant particle-particle attraction appears in this frequency regime. Nevertheless, the electrothermal flow is comparable with the MW induced repulsive force and turns more influential as the light intensity is elevated. The enhanced drag then contributes to the compact particle aggregation. Although the laser intensity induces toroidal flow – greater hydrodynamic drag to compact and lift particles, the hydrodynamic lift (F_l) may surpass the adhesive force (F_e) and removes particles from the surface at higher laser power. Taking all the onward results into consideration, the operating conditions were set for 16.5 V_{pp} and 69 W cm^{-2} at 5 kHz.

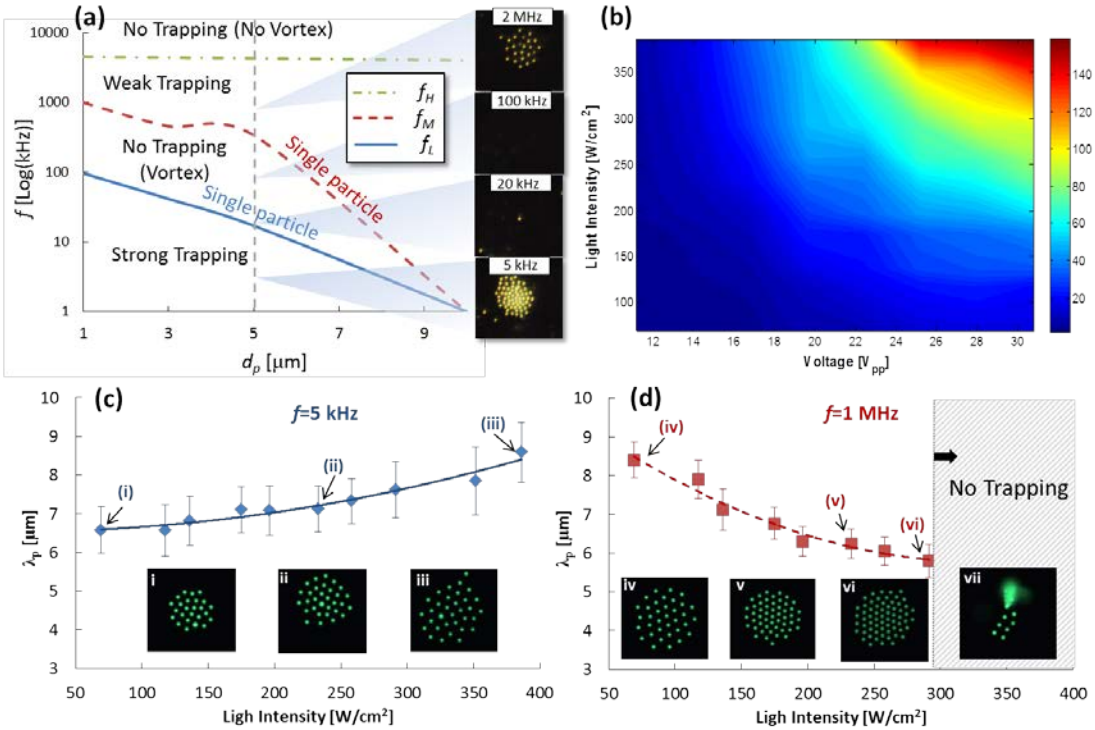

Fig. 5: *Characterizations of the optoelectrokinetic trapping. (a) Behavior of particles varies with frequency and particle size. (b) Surface contour of concentration efficiency of 5-μm particles as a function of laser intensity and voltage. The color bar represents the number of particles trapped within the irradiated spot in a second. (c) Mean distance between 5-μm particles with respect to light intensity at 5 kHz (n=3). The error bars represent standard deviations. (d) Mean distance between 5-μm particles with respect to light intensity at 1 MHz (n=3). The error bars represent standard deviations. The aggregation collapses when the light intensity exceeds 291 W cm^{-2}.*

Manipulation Schemes

The optoelectric microchip can perform several sophisticated particle manipulation operations. With the regular conditions mentioned previously, several manipulation capabilities, such as micro/nano-particle concentration, translation, single particle capturing, sorting, and patterning, were implemented by modulating frequency, path of irradiation, and voltage.[17-20, 29] The demonstrations show that the technique is not only excellent in dynamic concentration but also useful in other applications such as single cell manipulation and self-assembly.

Several representative manipulation capabilities are depicted in Fig. 6. Fig. 6a shows no trapping when the laser irradiation and electric fields are not simultaneously applied. In other words, only an electric field or a laser

beam acting on the microchip is incapable of producing successful trapping. However, when both laser irradiation and electric fields are applied simultaneously, particles can be rapidly concentrated within the irradiated spot as shown in Fig. 6b. That REP is a result of synergistic action of light and electric fields has been established earlier also[17, 29]. The extent of cluster can be altered by either increasing the laser intensity or the size of the irradiated spot. For translation, the trapped site was changed by simply moving the irradiated spot. Fig. 6c shows a transient status of a cluster translating from an old spot to a new one. Fig. 6d shows the successful trapping of 5-μm single particle at 17 kHz (also see Movie S5). As demonstrated previously, single particle trapping can be realized at transitional frequency. Despite fluid motion in its vicinity, the particle could be trapped stably.

Fig.s 6e and 6f show a realization of size-dependent sorting based on the frequency modulation (also see Movie S6). A mixture of 1 μm and 5 μm particle suspension was initially concentrated at a low frequency of 5 kHz. When the frequency was gradually elevated to 36 kHz, 5 μm particles firstly reached their relaxation threshold. Subsequently, 5 μm particles were released from the cluster while 1 μm particles remained trapped. The simple demonstration reveals insight to sort particles by size. Nevertheless, frequency modulation can be used to sort particle by type as well.[20]

When intentionally changing the voltage with irradiation, such as on-off the power or coupling the input signal with a DC shift, the trapped particles will be irreversibly stuck to the surface of electrode. By performing this operation with a careful arrangement, special patterns were achieved. Two types of operation were implemented. In Fig. 6g clusters of 5-μm particles were assembled step by step to form a letter "L" at 5 kHz. Similarly, in Fig. 6h single 5-μm particles were assembled step by step to form the same letter "L" at 17 kHz. This is the first application of REP for controlled patterning of single particles and has the potential to be useful for bottom-up manufacturing.

An attempt to aggregate nano-particles was also made successfully with the optoelectrokinetic technique as shown in Fig. 6i (also see Movie S7). 22-nm fluorescent polystyrene particles were suspended in DI water, making a conductivity of 0.3 mS m^{-1}. A cluster rapidly took shape after a laser beam and an electric field of 16.5 V_{pp} at 5 kHz were applied on the microchip simultaneously. Switching off either the electric field or the laser removed the cluster, implying a typical response of REP. Although aggregation of nano-particles using REP was demonstrated in the prior literature,[19] results herein demonstrate the smallest particle trapped with REP to date. All

of these manipulation capabilities therefore provide essential tools to realize the all-in-one bead-based bioassays. More detailed information regarding the sorting, patterning, and nano-particle concentration can also be referred to the prior literature.[17, 20, 29, 30]

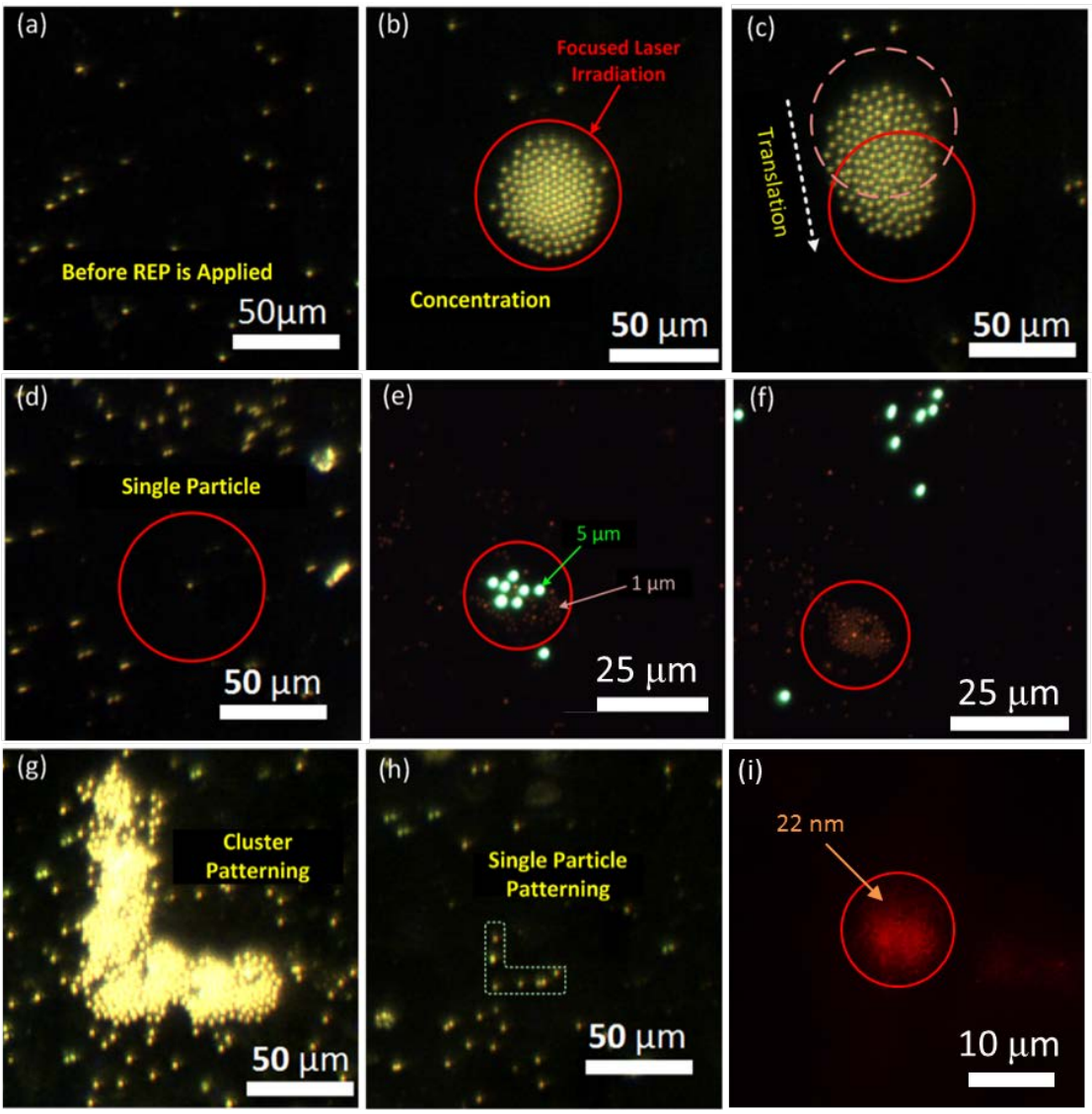

Fig. 6: *Repertoire of particle manipulation with the optoelectrokinetic technique: (a) no trapping in the initial state, (b) micro-particle aggregation at 5 kHz, (c) translation at 5 KHz, (d) single particle manipulation (d_p=5 µm) at 17 kHz, (e) 1-µm and 5-µm particles trapped simultaneously at 5 kHz, (f) sorting by size at 36 kHz, (g) patterning with clusters, (h) patterning with single particles, and (i) nano-particle aggregation at 5 kHz and 16.5 V_{pp}.*

Bead-based Signal Enhancement

Taking advantage of the optoelectrokinetic manipulation, the technique was used to enhance the output signal in a bead-based assay. Compared with conventional bioassays achieved with fixed and functionalized surfaces,[31, 32] bead-based assays feature high flexibility. The concept of the signal enhancement herein is as target samples tagged with fluorescence bind to a functionalized particle, the dilute signal can be concentrated in a defined region. By aggregating the dispersed particles conjugated with the tagged samples, the signal can be further improved. The extent of the aggregation is dependent on the irradiated area. Although a large aggregate can facilitate the detection, the light intensity per unit area decreases significantly as the irradiated area increases (see Fig. 5b). Therefore, the fluorescent signal will start to decline after the irradiated spot exceeds a threshold. Unless a higher power light source is used, compromised signal enhancement for each condition can be obtained by trial and error. Note that the current optoelectric technique can achieve only planar concentration, but three dimensional stacking of particles will further benefit the signal enhancement.

For a bioassay demonstration, the streptavidin-biotin binding reaction was chosen to assess the feasibility of signal enhancement by concentration. FITC tagged biotin represents a biomarker in a biological fluid while the streptavidin-conjugated particles represent a platform in an immunoassay. Dilute biotin-FITC solutions ranging from 3.87 pM to 387 μM were prepared. Each solution had a volume of 100 μL. In addition, streptavidin-conjugated particle suspension of 1.2×10^7 count mL^{-2} was prepared in a volume of 100 μL. By mixing the streptavidin and biotin suspensions at room temperature, the dispersed biotin would bind to the particles in a few seconds due to rapid mixing by the electrothermal flow. When the binding process was complete, a glow of green fluorescence from each particle could be clearly observed through a fluorescent microscope. When the particles were further concentrated by REP, the fluorescent signal was effectively elevated (Fig. 7a and also see Movie S8). Meanwhile, it was also found that the fluorescence was increased as more biotin molecules were allowed to bind on the surface of each particle by diluting the streptavidin-conjugated particle suspension (Fig. 7b). The result suggests that maintaining the concentration of functionalized particles lower than that of biomarkers is necessary to ensure all the binding sites on a particle are taken. Therefore, most biomarkers can be gathered in a specific region of interest instead of being dispersed in the whole medium.

To assess the effect of signal enhancement by the technique, a comparison between a commercial equipment, ELISA reader, and the optoelectric microchip was conducted (Fig. 7c). Pure DI water was treated as a blank in

each measurement. The minimal concentration was defined as the readout crosses over the blank. The result showed that the minimal concentration detected by the optoelectric device was 3.87 nM while the ELISA reader was only able to detect 387 nM. A signal enhancement of two orders of magnitude was made with the technique. Moreover, the signal was constantly improved as the functionalized particles were further diluted according to the result shown in the Fig. 7b. Direct evidences from the SEM images show that the surfaces of the functionalized particles were covered by matrix-like exogenous substances (Fig. 7d). The surfaces of the particles become very rugged when the particles are surrounded by more biotin molecules (from (i) to (vi)). Since only biotin-FITC was added in the suspension, a reasonable conjecture to the unknown substance turns out to be the biotin-FITC. The demonstration provides an insight to similar bioassays conducted in the same fashion. For biological reactions, proteins can survive at temperatures below 40 °C.[33-35] Considering the current technique is primarily driven by a temperature gradient peaking at 39 °C not an absolute temperature, an extension to immunoassays is therefore highly feasible.

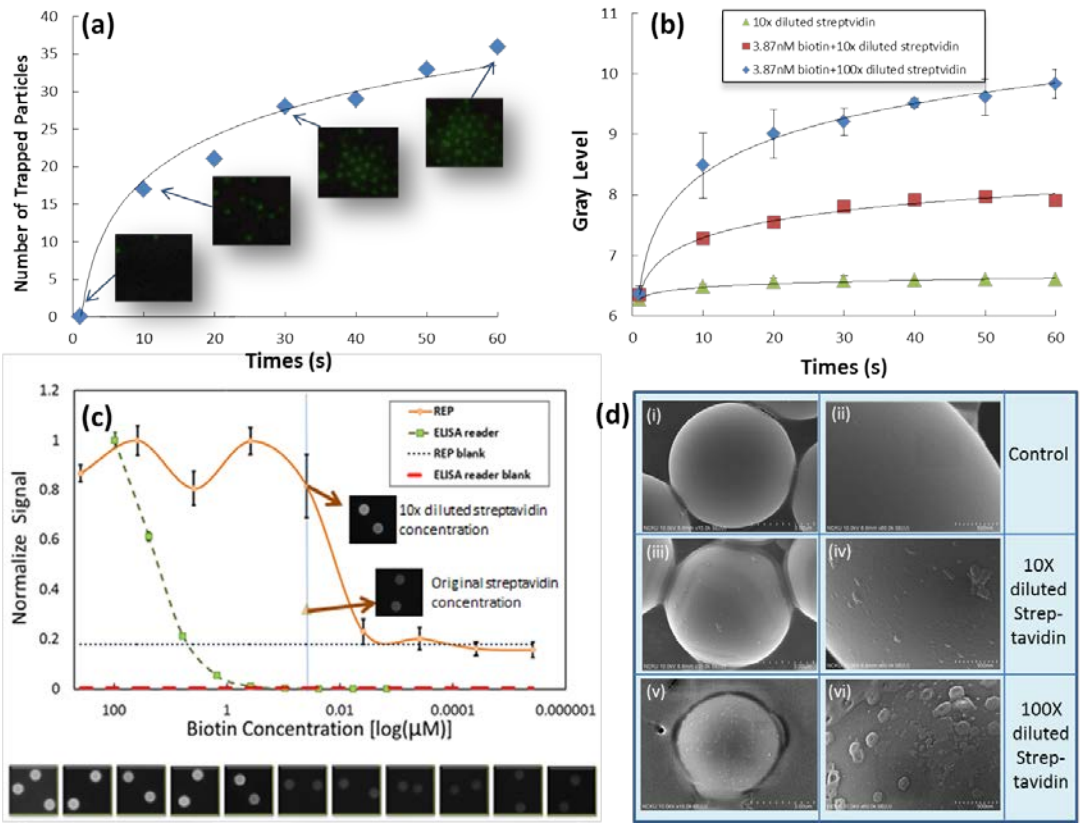

Fig. 7: *(a) The fluorescent signal is elevated when more particles are concentrated with time (n=1). (b) By diluting the functionalized particles, more biotin can bind to streptavidin. Note that each condition was measured three times (n=3)*

and the error bars represent standard deviations. (c) Signal is enhanced by concentrating functionalized particles based on the biotin-streptavidin reaction. The readout concentration of the optoelectric microchip is 3.87 nM (n=30) while that of ELISA reader is 387 nM (n=3). The error bars represent standard deviations. (d) SEM images of particles bound with and without biotin-FITC. Insets (ii), (iv), and (vi) are close-ups of insets (i), (iii), and (v), respectively.

Conclusion

In this paper, we present a powerful optoelectrokinetic technique for rapidly and dynamically manipulating particles. To facilitate analysis, an empirical model based on our observations and prior studies was created. Successful trapping occurred when laser irradiation and electric fields were simultaneously applied. The laser irradiation was used to generate electrohydrodynamic flow, dragging particles toward the center of irradiation. The AC electric field was used to induce electrokinetic effects on particles, such as particle-particle and particle-electrode interactions. When all forces were in equilibrium, particles steadily aggregated within the irradiated spot. Characterizations of the optoelectrokinetic technique indicated that the trapping is a function of frequency, voltage, laser intensity, and particle size. By modulating the frequency from 5 kHz to 5 MHz, all particles expressed distinct responses in different frequency domains as predicted in the model. The good agreement with the prediction also validated the model. Several fundamental manipulation capabilities were conducted by simply modulating frequency, path of irradiation, and voltage. Among them, particle concentration, translation, sorting and patterning were also reported in the prior studies.[17-20, 29] Nevertheless, it is noteworthy that three novel observations were firstly made herein, including (1) single particle trapping, (2) smallest nano-particle (22 nm) trapped by REP, and (3) re-aggregation phenomenon at high frequencies. The extended demonstrations provide insight to the concept of performing multiple tasks on a single device based on bead-based bioassays.

For an assessment, the technique was actually used to enhance the signal in a low-dose sample. Biotin-FITC and streptavidin-conjugated particles were used to represent a biomarker and a platform in an immunoassay, respectively. The specific binding reaction using the optoelectrokinetic technique showed a distinct signal improvement as compared with an ELISA reader. With different functionalized particles, we expect this technique to benefit more signal detections in the near future.

Acknowledgements

The authors are grateful to the grant 101-2221-E-006-024-MY2 funded by the Ministry of Science and Technology and the National Research Foundation of Korea (NRF) grant funded by the Korean government (MSIP) (No. NRF-2012K2A1A2033138) for supporting this work. This research also partially received funding from the Headquarters of University Advancement at the National Cheng Kung University, which is sponsored by the Ministry of Education, Taiwan.

Notes and references

**Corresponding author. E-mail: oswaldchuang@mail.ncku.edu.tw*

[a] *Department of Biomedical Engineering, National Cheng Kung University, Tainan, Taiwan. Tel: 06-2757575 ext 63433; Fax: 06-2343270;*

[b] *Medical Device Innovation Center, National Cheng Kung University, Tainan, Taiwan.*

[c] *Department of Mechanical Engineering, University of Alberta, Edmonton, Canada.*

[d] *Mechanical Engineering, University of Louisville, Louisville, U.S.A.*

[e] *Electronics and Computer Science, University of Southampton, Southampton, U.K.*

[f] *Mechanical Engineering, Pusan National University, Busan, South Korea*

† Electronic Supplementary Information (ESI) available: [details of any supplementary information available should be included here]. See DOI: 10.1039/b000000x/

‡ Footnotes should appear here. These might include comments relevant to but not central to the matter under discussion, limited experimental and spectral data, and crystallographic data.

[1] B. Teste, A. Ali-Cherif, J. L. Viovy and L. Malaquin, *Lab Chip*, 2013, **13**, 2344-2349.
[2] S. Miraglia, E. E. Swartzman, J. Mellentin-Michelotti, L. Evangelista, C. Smith, I. I. Gunawan, K. Lohman, E. M. Goldberg, B. Manian and P. M. Yuan, *J. Biomol. Screen.*, 1999, **4**, 193-204.
[3] D. Horejsh, F. Martini, F. Poccia, G. Lppolito, A. D. Caro and M. R. Capobianchi, *Nucl. Acids Res.* , 2005, **33**, e13.
[4] J. A. Thompson and H. H. Bau, *J. Chromatogr. B*, 2010, **878**, 228-236.
[5] X. Yu, M. Hartmann, Q. Wang, O. Poetz, N. Schneiderhan-Marra, D. Stoll, C. Kazmaier and T. O. Joos, *PLOS One*, 2010, **5**, e13125.
[6] J. N. Krishnan, C. Kim, H. J. Park, J. Y. Kang, T. S. Kim and S. K. Kim, *Electrophoresis*, 2009, **30**, 1457-1463.
[7] S. Agastin, M. R. King and T. B. Jones, *Lab Chip*, 2009, **9**, 2319–2325.

[8] Z. T. Kuo and W. H. Hsieh, *Sens. Actuators, B*, 2009, **141**, 293-300
[9] M. Javanmard, S. Emaminejad, R. W. Dutton and R. W. Davis, *Anal. Chem.*, 2011, **84**, 1432-1438.
[10] A. Ashkin, *Phys. Rev. Letts.*, 1970, **24**, 156-159.
[11] A. Ashkin, J. M. Dziedzic and T. Yamane, *Nature*, 1987, **330**, 769-771.
[12] K. M. Mayer, F. Hao, S. Lee, P. Nordlander and J. H. Hafner, *Nanotechnology*, 2010, **21**, 255503.
[13] A. Kumar, S. J. Williams, H. S. Chuang, N. G. Green and S. T. Wereley, *Lab Chip*, 2011, **11**, 2135-2148.
[14] A. U. L. Haque and A. Kumar, *Expert Rev. Mol. Diagn.*, 2012, **12**, 9-11.
[15] J. S. Kwon, S. P. Ravindranath, A. Kumar, J. Irudayaraj and S. T. Wereley, *Lab Chip*, 2013, **12**, 4955-4959.
[16] H. Hwang and J. K. Park, *Lab Chip*, 2011, **11**, 33-47.
[17] S. J. Williams, A. Kumar and S. T. Wereley, *Lab Chip*, 2008, **8**, 1879-1882.
[18] A. Kumar, H. S. Chuang and S. T. Wereley, *Langmuir*, 2010, **26**, 7656-7660.
[19] S. J. Williams, A. Kumar, N. G. Green and S. T. Wereley, *Nanoscale*, 2009, **1**, 133-137.
[20] S. J. Williams, A. Kumar, N. G. Green and S. T. Wereley, *J. Micromech. Microeng.* , 2010, **20**, 015022.
[21] A. Kumar, C. Cierpka, S. J. Williams, C. J. Kähler and S. T. Wereley, *Microfluid. Nanofluid.*, 2011, **10**, 355-365.
[22] J. Wong, A. Chilkoti and V. T. Moy, *Biomol. Eng.*, 1999, **16**, 45-55.
[23] N. G. Green, A. Ramos, A. González, A. Castellanos and H. Morgan, *J. Electrostat.*, 2001, **53**, 71-87.
[24] A. Kumar, S. J. Williams and S. T. Wereley, *Microfluid. Nanofluid.*, 2009, **6**, 637-646.
[25] W. D. Ristenpart, P. Jiang, M. A. Slowik, C. Punckt, D. A. Saville and I. A. Aksay, *Langmuir : the ACS journal of surfaces and colloids*, 2008, **24**, 12172-12180.
[26] W. D. Ristenpart, I. A. Aksay and D. A. Saville, *Phys. Rev. E*, 2004, **69**, 021405.
[27] W. D. Ristenpart, I. A. Aksay and D. A. Saville, *J. Fluid Mech.*, 2007, **575**, 83-109.
[28] M. T. Wei, J. Junio and H. D. Ou-Yang, *Biomicrofluidics*, 2009, **3**.
[29] A. Kumar, J. S. Kwon, S. J. Williams, N. G. Green, N. Yip and S. T. Wereley, *Langmuir*, 2010, **26**, 5262-5272.
[30] V. Velasco and S. J. Williams, *J. Colloid Interface Sci.*, 2013, **394**, 598-603.
[31] K. Toda, M. Tsuboi, N. Sekiya, M. Ikeda and K. I. Yoshioka, *Anal. Chim. Acta*, 2002, **463** 219-227.
[32] B. Su, J. Tang, H. Chen, J. Huang, G. Chen and D. Tang, *Anal. Methods*, 2010, **2**, 1702-1709.
[33] M. Kristiansen, M. K. Frøystad, A. L. Rishovd and T. Gjøen, *J. Gen. Virol.*, 2002, **83**, 2693–2697.
[34] D. L. Ingram, P. G. Webb and R. H. Biggs, *Plant Soil*, 1986, **96**, 69-76.
[35] A. Holmberg, A. Blomstergren, O. Nord, M. Lukacs, J. Lundeberg and M. Uhlén, *Electrophoresis*, 2005, **26**, 501-510.